Polymorphism analyses and protein modelling inform on functional specialization of Piwi clade genes in the arboviral vector *Aedes albopictus*

Short Title: Piwi clade genes of *Aedes albopictus*

Michele Marconcini[1], Luis Hernandez[1], Giuseppe Iovino[1], Vincent Houé[2], Federica Valerio[1], Umberto Palatini[1], Elisa Pischedda[1], Jacob Crawford[3], Rebeca Carballar-Lejarazu[1]*, Lino Ometto[1], Federico Forneris[1], Anna-Bella Failloux[2], Mariangela Bonizzoni[1&]

[1] Department of Biology and Biotechnology, University of Pavia, Italy
[2] Arbovirus and Insect Vectors Units, Department of Virology, Institut Pasteur, Paris, France
[3] Verily Life Sciences LLC, San Francisco, USA
* Current Address: University of California, Irvine, Department of Molecular Biology and Biochemistry, California, USA
[&] Corresponding author

Keywords

Aedes albopictus, piRNA pathway, arbovirus, development

Abstract

Current knowledge of the piRNA pathway is based mainly on studies on the model organism *Drosophila melanogaster*, where three proteins of the Piwi subclade of the Argonaute family interact with PIWI-interacting RNAs to silence transposable elements in gonadal tissues. In mosquito species that transmit epidemic arboviruses such as the Dengue and Chikungunya viruses, *Piwi* clade genes underwent expansion, are also expressed in the soma, and code for proteins that may elicit antiviral functions and crosstalk with other proteins of recognized antiviral mechanisms. These observations underline the importance of expanding our knowledge of the piRNA pathway beyond *D. melanogaster*.

Here we focus on the emerging arboviral vector *Aedes albopictus* and we couple traditional approaches of expression and adaptive evolution analyses with most current computational predictions of protein structure to study evolutionary divergence among Piwi clade proteins. Superposition of protein homology models indicate high structure similarity among all Piwi proteins, with high levels of amino acid conservation in the inner regions devoted to RNA binding. On the contrary, solvent-exposed surfaces showed low conservation, with several sites under positive selection. Expression profiles of *Piwi* transcripts during mosquito development and after infection with the Dengue 1 virus showed a concerted elicitation of all *Piwi* transcripts during viral dissemination, while the maintenance of infection primarily relied on the expression of *Piwi5*. In contrast, establishment of persistent infection by the Chikungunya virus is accompanied by an increased expression of all *Piwi* genes, particularly *Piwi4* and, again, *Piwi5*. Overall these results are consistent with functional specialization and a general antiviral role for *Piwi5*. Experimental evidences of sites under positive selection in *Piwi1/3*, *Piwi4* and *Piwi6*, further provide useful knowledge to design tailored functional experiments.

Author summary

Argonautes are ancient proteins involved in many cellular processes, including innate immunity. Early in eukaryote evolution, Argonautes separated into Ago and Piwi clades, which maintain a dynamic evolutionary history with frequent duplications and losses. The use of *Drosophila melanogaster* as a model organism proved fundamental to understand the function of Argonautes. However, recent studies showed that the patterns and observations made in *D. melanogaster*, including the number of Argonautes, their expression profile and their function, are a rarity among Dipterans.

In vectors of epidemic arboviruses such as Dengue and Chikungunya viruses, *Piwi* genes underwent expansion, are expressed in the soma, and some of them appear to have antiviral functions. Besides being an important basic question, the identification of which (and how) *Piwi* genes have antiviral functions may be used for the development of novel genetic-based strategies of vector control. Here we coupled population genetics models with computational predictions of protein structure and expression analyses to investigate the evolution and function of *Piwi* genes of the emerging vector *Aedes albopictus.* Our data support a general antiviral role for *Piwi5*. Instead, the detection of complex expression profiles with the presence of sites under positive selection in *Piwi1/3*, *Piwi4* and *Piwi6* requires tailored functional experiments to clarify their antiviral role.

Introduction

First discovered for their role in plant developmental, proteins of the Argonaute family have been found in all domains of life, where they are essential for a wide variety of cellular processes, including innate immunity [1,2].

Recent studies provided evidence of evolutionary expansion and functional divergence of Argonautes in Dipterans, including examples in both the Ago and Piwi subclades [3]. Differences in function and copy number have also been found in other taxa such as nematodes [4], oomycetes [5] and higher plants [6], indicating a dynamic evolutionary history of this protein family. In eukaryotes, Argonautes are key components of the RNA interference (RNAi) mechanisms, which can be distinguished in small interfering RNA (siRNA), microRNA (miRNA) and the PIWI-interacting RNA (piRNA) pathways.

The siRNA pathway is the cornerstone of antiviral defense in insects. The canonical activity of this pathway is the Argonaute 2 (Ago2)-dependent cleavage of viral target sequences. Ago2 is guided to its target through an RNA-induced silencing complex (RISC) loaded with 21-nucleotide (nt)-long siRNAs. siRNAs are produced from viral double-strand RNAs intermediates by the RNAase-III endonuclease activity of Dicer-2 (Dcr2) and recognize the target based on sequence complementarity [7]. Dcr2 also possesses a DExD/H helicase domain that mediates the synthesis of viral DNA (vDNA) fragments [8], which appear to further modulate antiviral immunity [8]. vDNA fragments are synthetized in both circular and linear forms, in complex arrangements with sequences from retrotransposons, but details of their mode of action have not been elucidated yet [8,9]. We and others recently showed that the genomes of *Aedes spp.* mosquitoes harbor fragmented viral sequences, which are integrated next to transposon sequences, are enriched in piRNA clusters and produced PIWI-interacting RNAs (piRNAs) [10,11]. The similar organization between vDNAs and viral integrations, along with the production of piRNAs of viral origin (vpiRNAs) following arboviral infection of *Aedes* spp. mosquitoes, led to the hypothesis that the piRNA pathway functions cooperatively with the siRNA pathway in the acquisition of tolerance to infection [10,12,13].

Current knowledge on the piRNA pathway in insects is based mainly on studies on *Drosophila melanogaster*, where three proteins of the Piwi subclade, namely Argonaute-3 (AGO3), PIWI and Aubergine (AUB), interact with piRNAs to silence transposable elements (TEs) in gonadal tissues [14]. Interestingly, the piRNA pathway of *D. melanogaster* does not have antiviral activity and no viral integrations have been detected [15]. Additional differences exist between the piRNA pathway of *D. melanogaster* and that of mosquitoes, suggesting that *D. melanogaster* cannot be used as a model to unravel the molecular crosstalk between the siRNA and piRNA pathways leading to antiviral immunity in *Aedes* spp. mosquitoes. For instance, in *Aedes aegypti,* Piwi subclade has undergone expansion with seven proteins (i.e. Ago3, Piwi2, Piwi3, Piwi4, Piwi5, Piwi6 and Piwi7), which are alternatively expressed in somatic and germline cells and interact with both endogenous piRNAs and vpiRNAs [12,16,17]. Gonadal- or embryonic-specific expression is found for *Piwi1/3* and *Piwi7*, respectively [16], while *Ago3*, *Piwi4*, *Piwi5* and *Piwi6* are highly expressed in the soma and in the *Ae. aegypti* cell line Aag2 and contribute to the production of transposon-derived piRNAs [16,18]. Ago3 and Piwi5 also regulate biogenesis of piRNAs from the replication-dependent histone gene family [19]. Production of vpiRNAs is dependent on Piwi5 and Ago3 during infection of Aag2 cells with the *Alphavirus* CHIKV, Sindbis and Semliki Forest viruses (SFV), but relies also on Piwi6 following infection with the *Flavivirus* DENV2 [18,20–22]. Piwi4 does not bind piRNAs and its knock-down does not alter vpiRNA production upon infection of Aag2 cells with either SFV or DENV2 [18,23]. On the contrary Piwi4 coimmunoprecipitate with Ago2, Dcr2, Piwi5, Piwi6 and Ago3, suggesting a bridging role between the siRNA and piRNA pathways [21]. Despite these studies support an antiviral role for the piRNA pathway in *Aedes* spp. mosquitoes, a major challenge is to uncover the distinct physiological roles of Piwi proteins, if any. In duplicated genes, the presence of sites under positive selection is usually a sign of the acquisition of novel functions [24]. Additionally, under the “arm-race theory”, rapid evolution is expected for genes with immunity functions because their products should act against fast evolving viruses [25].

Besides being an important basic question, the understanding of functional divergence among Piwi proteins has applied perspectives for the development of novel genetic-based methods

to control vector transmission. This is particularly relevant for mosquitos borne viruses, as several *Aedes* spp. species are expanding their spatial distribution and may contribute to disease outbreaks.

In recent years, the Asian tiger mosquito *Aedes albopictus* has emerged as a novel global arboviral threat, invading every continent except Antarctica from its native home range of South East Asia [26]. Because this species is a competent vector for a number of arboviruses such as chikungunya (CHIKV), dengue (DENV), yellow fever (YFV) and Zika (ZIKV) viruses, its establishment in temperate regions of the world fostered the re-emergence or the new introduction of these arboviruses [27]. For instance, Chikungunya outbreaks occurred in Italy in 2007 and 2017 [28,29]; France and Croatia suffered from autochthonous cases of Dengue and Chikungunya in several occasions since 2010 [30–33]; and dengue is re-emerging in some regions of the United States [34]. Despite its increasing public-health relevance, knowledge on *Ae. albopictus* biology and the molecular mechanisms underlying its competence to arboviruses are still limited in comparison to *Ae. aegypti*.

Here we elucidate the molecular organization, intraspecific polymorphism and expression of *Piwi* clade genes of *Ae. albopictus* in an evolutionary framework using a combination of molecular, population genomics and computational protein modelling approaches. We show that the genome of *Ae. albopictus* harbours seven *Piwi* genes, namely *Ago3*, *Piwi1/3*, *Piwi2*, *Piwi4*, *Piwi5*, *Piwi6* and *Piwi7*. For the first time in mosquitoes, we show sign of adaptive evolution in *Piwi1/3*, *Piwi4*, *Piwi5* and *Piwi6*, including sites in the MID and PAZ domains. Additionally, expression profiles during mosquito development and following infection with DENV or CHIKV support functional specialization of Piwi proteins, with a prominent and general antiviral role for the transcript of *Piwi5*.

Results

Seven *Piwi* genes are present in the genome of *Ae. albopictus*

Bioinformatic analyses of the current genome assemblies of *Ae. albopictus* (AaloF1) and the C6/36 cell line (canu_80X_arrow2.2), followed by copy number validation, confirmed the presence of seven *Piwi* genes (i.e. *Ago3*, *Piwi1/3*, *Piwi2*, *Piwi4*, *Piwi5*, *Piwi6* and *Piwi7*) in *Ae. albopictus* (S1

Table). Genomic DNA sequences were obtained for each exon-intron boundaries confirming in all *Piwi* genes the presence of the PAZ, MID and PIWI domains, the hallmarks of the Piwi subfamily of Argonaute proteins [35]. For *Ago3, Piwi1/3, Piwi2, Piwi4* and *Piwi6*, single transcript sequences that correspond to predictions based on the identified DNA sequences were retrieved (S1 Dataset). Sequencing results of the transcript from *Piwi5* showed a sequence 27 bp shorter than predicted on the reference genome, due to a 45bp gap followed by a 18b insertion, 110 and 333 bases after the ATG starting codon, respectively. This transcript still includes the PAZ, MID and PIWI domains. The presence of this transcript was further validated by northern-blot (Fig 1). For *Piwi7*, the transcript sequence also appears shorter than predicted (Fig 1). Alignment and phylogenetic analyses, in the context of currently annotated *Piwi* transcripts of Culicinae and Anophelinae mosquitoes, confirmed one-to-one orthologous pairing between *Ae. albopictus Piwi* gene transcripts and those of *Ae. aegypti* (S2 Table, S1 Fig). Interestingly, *Piwi5*, *Piwi6* and *Piwi7* transcripts group together and appear more similar to one of the two Aubergine-like transcripts annotated in different Anophelinae species than to *Aedes Piwi2*, *Piwi1/3* and *Piwi4* transcripts. Regarding the latter, *Piwi2* and *Piwi1/3* form a species-specific clade, rather than follow a speciation pattern. Independent duplication events in *Ae. aegypti* and *Ae. albopictus*, followed by convergent functional evolution, is unlikely if we consider the presence of orthologues in more distant species. Rather, the two genes, which based on *Ae. aegypti* chromosomal map on chromosome 1 and are ~20 kb apart [17], may be undergoing inter-locus gene conversion via nonreciprocal recombination, which result in between-loci homogenization.

***Piwi* genes display high levels of polymorphism across populations and show signs of adaptive evolution**

Across *Drosophila* phylogeny, genes of the piRNA pathway display elevated rates of adaptive evolution [36], with rapidly evolving residues not clustering at the RNA binding site, but being distributed across the proteins [3]. The RNA binding site is found within the PAZ domain, at the amino-terminal part of Piwi proteins [35,37]. The PIWI domain resides on the opposite side, at the carboxyl terminus. The PIWI domain belongs to the RNase H family of enzymes and the catalytic site is formed by three conserved amino acids (usually aspartate-aspartate-glutamate, DDE, or

aspartate-aspartate-histidine, DDH) [35,38]. Between the PAZ and PIWI domains there is the MID domain. MID specifies strand- and nucleotide-biases of piRNAs, including their Uridine 5' bias [39,40]. To evaluate the selective pressures acting along these genes, we analysed the polymorphism pattern in *Ae. albopictus* samples from wild-collected populations and from the Foshan reference strain. Synonymous and non-synonymous mutations were found for each gene in all populations (Fig 2), with *Piwi1/3* displaying the lowest polymorphism (Table 1).

Table 1. Polymorphism of *Aedes albopictus Piwi* genes in mosquitoes from the Foshan strain and wild-caught mosquitoes from La Reunion (Reu) and Mexico (Mex). We report the number of sequences (*n*), as well as the number of sites (*L*), segregating sites (*S*), polymorphism measured as π and θ, and the Tajima's *D* statistic for both synonymous (s) and non-synonymous sites (a) for each gene and population (and for the pooled sample).

	n	*L*	L_s	L_a	S_s	S_a	π_s	π_a	θ_s	θ_a	π_a/π_s	D_s	D_a
Ago3													
Pooled	112	2832	680.2	2151.8	316	19	0.0699	0.0005	0.0878	0.0017	0.007	-0.68	-1.95
Foshan	32	2832	680.1	2151.9	124	5	0.0559	0.0004	0.0453	0.0006	0.007	0.89	-0.82
Mex	48	2832	680.2	2151.8	253	14	0.0780	0.0007	0.0838	0.0015	0.009	-0.25	-1.60
Reu	32	2658	643.8	2014.2	189	4	0.0678	0.0002	0.0729	0.0005	0.003	-0.27	-1.50
Piwi1-3													
Pooled	112	2658	644.3	2013.7	136	23	0.0319	0.0010	0.0399	0.0022	0.033	-0.66	-1.51
Foshan	32	2658	644.0	2014.0	10	2	0.0047	0.0003	0.0039	0.0002	0.064	0.68	0.44
Mex	48	2658	644.9	2013.1	117	21	0.0463	0.0017	0.0409	0.0024	0.037	0.48	-0.89
Reu	32	2658	643.8	2014.2	52	4	0.0188	0.0004	0.0201	0.0005	0.021	-0.23	-0.48
Piwi2													
Pooled	112	2625	644.0	1981.0	242	28	0.0760	0.0012	0.0710	0.0027	0.016	0.23	-1.65
Foshan	32	2625	644.0	1981.0	115	10	0.0663	0.0017	0.0443	0.0013	0.026	1.88	1.11
Mex	48	2625	643.9	1981.1	184	15	0.0823	0.0010	0.0644	0.0017	0.012	1.01	-1.28
Reu	32	2625	644.1	1980.9	151	6	0.0712	0.0005	0.0582	0.0008	0.007	0.85	-0.94
Piwi4													
Pooled	112	2592	620.0	1972.1	268	61	0.0729	0.0025	0.0817	0.0058	0.034	-0.36	-1.82
Foshan	32	2592	620.1	1971.9	122	18	0.0610	0.0009	0.0489	0.0023	0.015	0.94	-2.05
Mex	48	2592	619.8	1972.2	181	41	0.0692	0.0035	0.0658	0.0047	0.051	0.19	-0.87
Reu	32	2592	620.1	1971.9	161	45	0.0699	0.0029	0.0645	0.0057	0.041	0.32	-1.79
Piwi5													
Pooled	112	2745	653.1	2091.9	148	23	0.0457	0.0016	0.0428	0.0021	0.035	0.22	-0.66
Foshan	32	2793	664.5	2128.5	58	8	0.0361	0.0018	0.0217	0.0009	0.050	2.47	2.78

Mex	48	2745	652.9	2092.1	137	13	0.0470	0.0017	0.0473	0.0014	0.036	-0.02	0.65
Reu	32	2793	663.4	2129.6	89	6	0.0326	0.0008	0.0333	0.0007	0.025	-0.08	0.40
Piwi6													
Pooled	112	2661	649.0	2012.0	242	8	0.0805	0.0010	0.0705	0.0008	0.013	0.47	0.82
Foshan	32	2661	648.3	2012.8	92	3	0.0632	0.0001	0.0352	0.0004	0.002	2.99	-1.69
Mex	48	2661	649.9	2011.1	213	7	0.0840	0.0001	0.0739	0.0008	0.001	0.50	-2.33
Reu	32	2661	648.5	2012.5	163	4	0.0784	0.0001	0.0624	0.0005	0.001	0.98	-2.01
Piwi7													
Pooled	112	1977	469.8	1507.2	192	33	0.0877	0.0036	0.0772	0.0041	0.041	0.45	-0.42
Foshan	32	1977	469.8	1507.2	118	15	0.0905	0.0034	0.0624	0.0025	0.038	1.71	1.25
Mex	48	1977	469.9	1507.1	150	23	0.0905	0.0034	0.0719	0.0034	0.038	0.93	-0.04
Reu	32	1977	469.6	1507.5	137	17	0.0803	0.0030	0.0724	0.0028	0.037	0.41	0.24

As expected, the laboratory strain Foshan showed the lowest levels of variability and Tajima's *D* values that contrast (in sign) from those of the other populations and from the pooled sample, consistent with a strong bottleneck associated to the strain establishment. In *Piwi4*, between 20 and 80 non-synonymous variants could be found inside and in proximity of the PAZ, MID and PIWI domains (S2 Fig.A), ten of these mutations were shared across all populations (S3 Table). The 5' region of *Piwi5* harboured several indels: two in-frame variants (i.e. 94_99del; 113_118del) were shared across all populations and were present in homozygosity in at least one sample (S2 Fig.B), suggesting that they are not detrimental. *Ago3* and *Piwi6* have very low non-synonymous nucleotide diversity, suggesting strong constraints at the protein level. However, the McDonald-Kreitman test [41] found signatures of adaptive evolution in *Piwi1/3* and also in *Piwi6*, consistent with divergent positive selection followed by purifying selection (Table 2.A). In contrast, *Piwi4* has a significant deficit of non-synonymous substitutions and/or excess of polymorphic non-synonymous segregating sites (Table 2.A). In this gene, Tajima's *D* is negative but in line with the values of the other *Piwi* genes, and the high non-synonymous polymorphism may reflect selection of intraspecific diversifying selection, as expected in genes involved in immunity. Because positive selection may have acted at the level of very few sites, this not contributing to the gene-level non-synonymous substitution pattern, we explicitly tested models of codon evolution. Signs of positive selection were found at different sites, including one site in the Linker2 and one site in the MID domain of *Piwi1/3*, two sites in the PAZ domain of *Piwi4*, two sites in the Flex domain of *Piwi5* and three sites, two in the Flex and

one in the Linker2 domains, of *Piwi6* (Table 2.B). Haplotype reconstruction of our samples showed that these mutations can co-occur on the same gene, with the only exception of Y278D+H287P in Piwi4 and A67P+G86S in *Piwi6*.

Table 2. **Insights into Evolutionary divergence of Piwi genes in *Ae. albopictus*.** A) McDonald-Kreitman test for each *Piwi* gene using the orthologous sequences of *Ae. aegypti* as outgroup. NI = Neutrality Index; Alpha = proportion of base substitutions fixed by natural selection; *P* estimated using Fisher's exact test. B) Output of Codeml with significant results regarding sites under positive selection.

A. McDonald-Kreitman test

	Ago3	***Piwi1/3***	***Piwi2***	***Piwi4***	***Piwi5***	***Piwi6***	***Piwi7***
NI	0.582	0.516	0.9	3.888	0.696	0.154	0.745
alpha	0.418	0.484	0.1	-2.888	0.304	0.846	0.255
P	0.114	0.008	0.785	< 0.001	0.18	< 0.001	0.272

B. Codeml output for sites under positive selection

Gene	Position[1]	Reference>Mutant[2]	P[3]	Domain[4]
AGO3	-	-	-	
Piwi1-3	485	K>R	0.965*	Linker2
	548	M>I	0.984*	MID
Piwi2	-	-	-	
Piwi4	278	Y>D	0.993**	PAZ
	287	H>A,D,P,V	1.000**	PAZ
Piwi5	89-90	SA>PT	1.000*	Flex
	139	T>A	1.000*	Flex
Piwi6	67	A>P	0.992**	Flex
	86	G>R,S	0.957*	Flex
	258	V>I	0.999**	Linker2
Piwi7	-	-	-	

[1] sites where signs of positive selection (ω > 1) were found; [2] reference amino acid and alternative missense variant; [3]probability that ω > 1 under the Bayes empirical Bayes (BEB) method (* = P > 0.95; ** = P > 0.99); [4]protein domain based on computational

predictions of molecular structures. Domains are as follows: Linker2, linker region between PAZ and MID; PAZ domain; MID domain; and Flex, the Flexible stretch at the N-terminus.

Finally, to gain insight on how variable *Piwi* genes are in comparison to slow- and fast-evolving genes of *Ae. albopictus*, we collected variability data of sets of genes previously identified to have slow and high evolutionary rates [42]. For each population, we compared the overall level of polymorphism (LoP) of the *Piwi* genes and of a dataset of fast-evolving genes (FGs) to that measured for a dataset of slow-evolving genes (SGs) (Pischedda et al., 2019). Our results indicate that *Piwi4*, *Piwi6* and *Piwi7* have LoP values comparable to those of FGs, while *Ago3* and *Piwi5* do not significantly deviate from the LoP values of SGs. Piwi1/3 appears to be conserved (Fig 3).

Computational predictions of molecular structures

The functional significance of the mutations under selection, as well as that of all the shared missense mutations in the PAZ and PIWI domains, was tested by computing predictions of three-dimensional molecular structures of the Piwi proteins using the most-recent X-ray crystallography structure of Argonaute proteins as templates [43,44]. Homology modelling revealed high structural conservation among the seven Piwi proteins despite sequence heterogeneity (S2 Fig.; Fig 4.A).

Similarly, to *D. melanogaster,* the highest levels of amino acid sequence conservation were found in the regions that, based on homology modelling, define the inner pocket of Argonaute molecular assembly where the RNA binds. Significantly lower sequence conservation was found on the proteins surface (Fig 4.B). Based on our computational predictions, we could not detect aminoacidic polymorphisms that would affect RNA binding or processing, suggesting that all *Ae. albopictus* Piwi proteins may retain the Argonaute-like functions. Mapping of mutations under positive selection (Table 2.B) on the homology models showed that all variant amino acids were in regions distant from the predicted RNA-binding and/or processing sites, suggesting that these mutations are unlikely to alter protein folding, but could influence its stability.

Developmental profile of *Ae. albopictus Piwi* genes

To further gain insights on the functional specialization of *Piwi* genes, we assessed their expression profile throughout mosquito development, namely at 4-8 hours (h) after deposition to

capture the maternal-zygotic transition in expression, at late embryogenesis (i.e. 12-16 h and 16-24 h post deposition), at two time points during larval development (i.e. 1st and 4th instar larvae) and at pupal and adult stages (for the latter only we sampled separately males and females). Adult females were dissected to extract ovaries from the carcasses both from females kept on a sugar diet and 48 h after a blood meal, when a peak in *Piwi* gene expression was previously observed [45].

Expression levels of *Ago3*, *Piwi4*, *Piwi5*, *Piwi6* and *Piwi7* are at their peak in the embryonic stages, although at different time points (Fig 5). Overall, *AGO3*, *Piwi1/3, Piwi2* and *Piwi6* have a similar trend during development showing a second peak of expression in adult females and their ovaries, while the expression levels of *Piwi4*, *Piwi5* and *Piwi7* remain constant. In details, *Piwi7* is mostly expressed 4-8h after deposition*, Piwi5* and *Piwi6* are mostly expressed after 8-16h and *Ago3* and *Piwi4* have their pick of expression at 16-24h. On the contrary, *Piwi1/3* and *Piwi2* are mostly expressed in ovaries extracted from blood-fed and sugar-fed females, respectively (Fig 5.A, S4.A table). Interestingly, when considering the absolute expression levels, *Piwi7* is the least expressed of all the genes at any tested time point, with limited expression seen only in embryos within 24 hours post deposition (i.e. Ct values for *Piwi7* ranged from 24.04 to 30.65, at 4-8h and 1st instar larvae, respectively; at the same time points, Ct values for *AGO3* were 27.45 and 26.96.). These results are consistent with lack of expression from published RNA-seq data from adult mosquitoes.

Overall, at the adult stages, *Ago3* and all *Piwi* genes were more expressed in females than males. Expression in ovaries was higher than in the corresponding carcasses, in both sugar- and blood-fed females. Differences in carcasses vs. ovaries expression were more pronounced after blood-meal for *Ago3*, *Piwi1/3* and *Piwi6,* while expression of *Piwi2* was doubled in sugar-fed *vs.* blood-fed ovaries.

***Piwi* genes expression following viral infection**

Finally, we assessed whether the expression pattern of *Piwi* genes was altered upon DENV and CHIKV infection (Fig 5.B). Clear differences in the expression pattern of *Piwi* genes was seen both when comparing data from CHIKV- *versus* DENV-infected samples, and carcasses *versus* ovaries. In ovaries, during CHIKV infection all *Piwi* genes were significantly up-regulated compared

to both sugar- and blood-fed mosquitoes. Four days post infection (dpi), the expression of *Ago3*, *Piwi1/3*, *Piwi6* and *Piwi7* was between 4 to 10 folds higher than that of *Piwi2*, *Piwi4* and *Piwi5*, which nevertheless were upregulated with respect to ovaries of sugar- and blood-fed mosquitoes. An opposite profile was seen in the carcasses, where all *Piwi* genes, particularly *Piwi1/3* and *Piwi4*, were down-regulated. At 4 dpi, CHIKV has already disseminated throughout the mosquito body, has reached the salivary glands and is able to be transmitted. CHIKV viral titer was reduced ten folds by 14 dpi and the profile of *Piwi* genes changed. Expression in the ovaries decreased between 3 (*Piwi5*) to 20 (*Piwi7*) times with respect to values observed at 4 dpi, but remained higher than the corresponding expression values in ovaries of both sugar and blood-fed mosquitoes. In carcasses all *Piwi* genes inverted their expression pattern during the infection phase, increasing up to more than 100 times in the case of *Piwi4*, *Piwi5* and *Piwi6.* At 14 dpi, expression of the *Piwi* genes was highest in CHIKV infected carcasses than in carcasses of sugar- and blood-fed mosquitoes.

For DENV, infection progresses differently than CHIKV. At 4 dpi there is no virus in the salivary gland, where the viral titer was measured at zero. By 21 dpi, DENV has established persistent infection [46]. At 4 dpi expression of *Piwi* genes was lower in DENV- and blood-fed ovaries than in ovaries of sugar-fed mosquitoes. The only exception was *Piwi6*, which was slightly up-regulated in ovaries of DENV-infected samples, but slightly down-regulated in ovaried of blood-fed mosquitoes. On the contrary, at the same time point, carcasses of DENV-infected samples showed a drastic increase in the expression of all *Piwi* genes with respect to blood-fed samples; this increase was between 7 to 87 times for *Piwi7* and *Piwi2,* respectively. By 21 dpi, expression in the ovaries increased for all *Piwi* genes, in comparison to what observed both at 4dpi and in blood-fed ovaries, suggesting the increase in expression of *Piwi* genes is related to DENV dissemination. Interestingly, if we compare levels of expression in CHIKV-infected ovaries at 4 dpi and DENV-infected samples at 21 dpi, corresponding to the time at which both viral species have disseminated throughout the mosquito body, we observe similar levels of fold-change expression of *Piwi4* and *Piwi7*, while *Ago3*, *Piwi1/3* and *Piwi6* show higher fold-change in CHIKV compared to DENV samples. Whether this trend is dependent on the viral species or viral titer requires further investigation. The same type of comparison in carcasses shows a higher fold-change expression level of all *Piwi* genes, particularly

Piwi1/3 and *Piwi5*, in DENV- *versus* CHIKV-infected samples, even if viral titer are lower for DENV (S4.B Table). Overall these results support the hypothesis of a concerted activity of all PIWI proteins during viral dissemination for DENV, and maintenance of infection rely on expression of primarily *Piwi5*. On the contrary, establishment of persistent CHIKV infection was accompanied by elicitation of all *Piwi* gene expression, particularly *Piwi4* and, again, *Piwi5*.

Discussion

Recent experimental evidences extend the function of the piRNA pathway to antiviral immunity in *Aedes spp.* mosquitoes [12,15]. The broader roles of the piRNA pathway in *Aedes* spp. mosquitoes, compared to what is known in *D. melanogaster*, has been linked to the expansion and functional specialization of its core components [12,47,48]. Besides *Ago3*, the genome of *Ae. aegypti* harbours six *Piwi* genes (i.e. *Piwi1/3, Piwi2, Piwi4, Piwi5, Piwi6, Piwi7),* some of which show tissue and development-specific expression profile and have been preferentially associated with either TE-derived or viral piRNAs [16,20,21]. These studies were based on the knowledge of the gene structure of each *Ae. aegypti Piwi* gene and the application of *ad hoc* RNAi-based silencing experiments and *in vitro* expression assays, but lacked an evolutionary perspective [18–21].

In this work we focused on the emerging arboviral vector *Ae. albopictus* and we show how the application of evolutionary and protein modelling techniques helps to unravel functional specialization of Piwi proteins. The genome of *Ae. albopictus* harbors one copy of *Ago3* and six *Piwi* genes (i.e. *Piwi1/3, Piwi2, Piwi4, Piwi5, Piwi6 and Piwi7*), each a one-to-one orthologue to the *Ae. aegypti Piwi* genes. The only exceptions are *Piwi2* and *Piwi1/3*, where the two genes from the same species cluster together. In *Ae. aegypti*, these two genes both map on Chromosome 1, separated by ~ 20kb, suggesting they may undergo frequent gene conversion.

All transcripts retain the PAZ and PIWI domains, which are the hallmarks of the Argonaute protein family [35]. By using homology modelling, we obtained predictions of molecular architectures for *Ae. albopictus Ago3* and *Piwi* proteins, onto which we mapped the putative boundaries of each domain. Superpositions and sequence comparisons allowed clear identification of the catalytic DDH

326 triad within the PIWI domain of all modelled proteins. This conservation is consistent with strong
327 sequence matching in the putative RNA binding regions of the PIWI, PAZ and MID domains and
328 suggests the possible maintenance of slicer activity, albeit experimental validation of each isoform
329 is necessary.

330 The expression of all *Piwi* genes was confirmed throughout the developmental stages and
331 the adult life of the mosquito, both in ovaries and somatic tissues. Interestingly, *Piwi7* transcript
332 expression starkly drops following early embryogenesis, to the point that we could detect it neither
333 in RNA-seq analyses, nor in Northern-blot experiments (data not shown).

334 The expression of *Piwi* genes was elicited upon arboviral infection, indirectly confirming the
335 antiviral role of the piRNA pathway. The expression profile of *Piwi* genes showed differences
336 depending on both the species of infecting virus and on when the expression was measured. In
337 CHIKV-infected samples, expression of *Piwi* genes was mostly elicited in ovaries or carcasses at 4
338 or 21 dpi, respectively. On the contrary, in DENV-infected samples, the highest expression of *Piwi*
339 genes was seen in carcasses 4 dpi. These results are concordant with the timing in piRNAs
340 accumulation following CHIKV or DENV infection. In *Ae. albopictus* mosquitoes infected with CHIKV,
341 secondary piRNAs are not found 3 dpi, but are enriched 9 dpi [9]. In contrast, in *Ae. aegypti*
342 mosquitoes infected with DENV2, piRNAs are the dominant small RNA populations 2 dpi [48].
343 Overall, these observations and our expression analyses support the hypothesis of an early
344 activation of the piRNA pathway following DENV infection, but a late activation after CHIKV infection.
345 Additionally, our expression analysis is consistent with a generalist antiviral role for Piwi5, which is
346 elicited both during DENV and CHIKV infection [20], but suggest a more prominent role for Piwi6
347 and Piwi1/3 or Piwi4 and Ago3 during infection with DENV and CHIKV, respectively.

348 # Materials and methods

349 ## Mosquitoes

350 *Aedes albopictus* mosquitoes of the Foshan strain were used in this study [10]. Mosquitoes
351 were reared under constant conditions, at 28 °C and 70-80% relative humidity with a 12/12 h

light/dark cycle. Larvae were reared in plastic containers at a controlled density to avoid competition for food. Food was provided daily in the form of fish food (Tetra Goldfish Gold Colour). Adults were kept in 30 cm^3 cages and fed with cotton soaked in 0.2 g/ml sucrose as a carbohydrate source. Adult females were fed with defibrinated mutton blood (Biolife Italiana) using a Hemotek blood feeding apparatus. Mosquitoes from Mexico and La Reunion island were collected in 2017 as adults and maintained in ethanol 70% before shipment to Italy. All samples were processed at the University of Pavia.

Mosquito infections

Foshan mosquitoes were infected with either DENV serotype 1, genotype 1806 or with CHIKV 06.21. DENV-1 (1806) was isolated from an autochthonous case from Nice, France in 2010 [49]. CHIKV 06-21 was isolated from a patient on La Reunion Island in 2005 [50]. Both strains were kindly provided by the French National Reference Center for Arboviruses at the Institut Pasteur. CHIKV 06-21 and DENV-1 1806 were passaged twice on cells to constitute the viral stocks for experimental infections of mosquitoes, on C6/36 cells for CHIKV 06-21 and on African green monkey kidney Vero cells for DENV-1 1806. Viral titers of stocks were estimated by serial dilutions and expressed in focus-forming units (FFU)/mL.

Four boxes containing 60 one-week-old females were exposed to an infectious blood-meal composed by 2 mL of washed rabbit red blood cells, 1 mL of viral suspension and 5 mM of ATP. The titer of the blood-meal was 10^7 PFU/mL for CHIKV and $10^{6.8}$ PFU/mL for DENV. Fully engorged females were placed in cardboard boxes and fed with a 10% sucrose solution. Mosquitoes were incubated at 28 °C until analysis.

In parallel, mosquitoes were fed with uninfected blood-meal or kept on a sugar-diet and grown in the same conditions. Thirty mosquitoes were killed to be analyzed at days 4 and 14 post-infection (pi) for CHIKV, and at days 4 and 21 dpi for DENV.

To estimate transmission, saliva was collected from individual mosquitoes as described in [51]. After removing wings and legs from each mosquito, the proboscis was inserted into a 20 µL tip containing 5 µL of Fetal Bovine Serum (FBS) (Gibco, MA, USA). After 30 min, FBS containing saliva

was expelled in 45 µL of Leibovitz L15 medium (Invitrogen, CA, USA) for titration. Transmission efficiency refers to the proportion of mosquitoes with infectious saliva among tested mosquitoes (which correspond to engorged mosquitoes at day 0 pi having survived until the day of examination). The number of infectious particles in saliva was estimated by focus fluorescent assay on C6/36 *Ae. albopictus* cells. Samples were serially diluted and inoculated into C6/36 cells in 96-well plates. After incubation at 28°C for 3 days (CHIKV) or 5 days (DENV), plates were stained using hyperimmune ascetic fluid specific to CHIKV or DENV-1 as primary antibody. A Fluorescein-conjugated goat anti-mouse was used as the second antibody (Biorad). Viral titers were 16,266±50,446 FFU and 155±125 FFU for CHIKV at 14 dpi and DENV at 21 dpi, respectively.

At the same time points mosquitoes that had been fed a not-infectious blood or kept on a sugar diet were sampled and dissected as above.

Bioinformatic identification of *Piwi* genes in the *Ae. albopictus* genome

The sequences of the *Ae. aegypti Piwi* genes [52] were used as query to find orthologs in the reference genome of the *Ae. albopictus* Foshan strain (AaloF1 assembly) and in the genome of the *Ae. albopictus* C6/36 cell line (canu_80X_arrow2.2 assembly) using the BLAST tool in Vectorbase (www.vectorbase.org). Inferred coding sequences (CDS) where analysed in Prosite (Prosite.expasy.org/prosite.html) to screen for the typical PAZ and PIWI domains of Argonaute proteins [53].

Copy number of *piwi* genes

qPCR reactions were performed using the QuantiNova SYBR Green PCR Kit (Qiagen) following the manufacturer's instructions on an Eppendorf Mastercycler RealPlex4, on genomic DNA from four mosquitoes and using gene-specific primers, after having verified their efficiency (S5Table). DNA was extracted using DNA Isolation DNeasy Blood & Tissue Kit (Qiagen). Estimates of gene copy number were performed based on the $2^{-\Delta CT}$ method using *Piwi6* and the para sodium channel genes (AALF000723) as references [54].

Structure of *Piwi* genes

DNA extracted from whole mosquitoes and dissected ovaries [55] was used as template in PCR amplifications to confirm the presence and the genome structure of each bioinformatically-identified *Piwi* gene. Primers were designed to amplify each exon, with particular attention to detect differences between paralogous *Piwi* genes (S1 Table). The DreamTaq Green PCR Master Mix (Thermo Scientific) was used for PCR reactions with the following parameter: 94 °C for 3 minutes, 40 cycles at 94 °C for 30 sec, 55 °C-62 °C for 40 sec, 72 °C for 1-2 minutes and final extension step of 72 °C for 10 minutes. PCR products were visualized under UV light after gel electrophoresis using 1-1.5% agarose gels stained with ethidium bromide and a 100 bp or 1 kb molecular marker. PCR products were either directly sequenced or cloned using the TOPO® TA Cloning® Kit strategy (Invitrogen) following the manufacturer's instructions. DNA plasmids were purified using the QIAprep Spin Miniprep Kit and sequenced.

Piwi gene transcript sequences and phylogeny

RNA was extracted using a standard TRIzol protocol from pools of 5 adult female mosquitoes to verify the transcript sequence of each *Piwi* gene. Sets of primers were designed for each gene to amplify its entire transcript sequence (S5 Table). PCR reactions were performed using a High Fidelity taq-polymerase (Platinum SuperFi DNA Polymerase, Invitrogen) following manufacturer's instructions. PCR products were cloned using the TOPO® TA Cloning® Kit (Invitrogen) and plasmid DNA, purified using the QIAprep Spin Miniprep Kit, was sequenced. Rapid amplification of cDNA ends (RACE) PCRs were performed using FirstChoice RLM-RACE Kit (Thermo Fisher Scientific) to analyse 5' and 3' ends of the transcript sequences following manufacturer's instructions. Amplification products were cloned and sequenced as previously indicated.

Sequences of the identified *Ae. albopictus Piwi* gene transcripts were aligned to sequences of *Culicidae* and *D. melanogaster Piwi* transcripts, as downloaded from VectorBase (www.vectorbase.org), using MUSCLE [56]. Maximum-likelihood based phylogenetic inference was based on RAxML after 1000 bootstrap resampling of the original dataset and was done through the

CIPRESS portal (http://www.phylo.org/index.php/). Resulting tree was visualised using FigTree (http://tree.bio.ed.ac.uk/software/figtree/).

Northern Blot analysis

10µg of total RNA from a pool of 10 sugar-fed females was run in a 1% x 2% agarose/formaldehyde gel (1 g agarose, 10 ml 10x MOPS buffer, 5.4 ml 37% formaldehyde, 84.6 ml DEPC water). Gels were washed twice in 20x SSC for 15 minutes prior to blotting. RNA was transferred to an Amersham Hybond-N+ nylon membrane (GE healthcare) using 20x SSC and cross-linked using UV light exposure for 1 minute. Probes were labelled with biotin using Biotin-High Prime (Roche). Hybridization and detection of biotinylated probes was performed using the North2South™ Chemiluminescent Hybridization and Detection Kit (Thermo Fisher Scientific) following manufacturer instructions.

Polymorphisms of *Piwi* genes

We investigated *Piwi* gene polymorphism by looking at the distribution of single nucleotide polymorphism in whole genome sequence data from total of 56 mosquitoes, of which 24 from Mexico, 16 from the island of La Reunion island and 16 from the reference Foshan strain. Whole genome sequencing libraries were generated and sequenced on the Illumina HiSeqX platform at the Genomics Laboratory of Verily in South San Francisco, California to generate 150 basepair paired-end reads.

Illumina reads were mapped to *Piwi* gene transcript sequences using Burrows-Wheeler Aligner (BWA-MEM) [57] with custom parameters. Polymorphisms was tested by Freebayes [58]. Annotation of the detected mutations, as well counts of synonymous and non-synonymous variants, were performed in snpEff [59]. Frameshifts and non-synonymous variants were plotted using muts-needle-plot [60]. Venn diagrams of positions with mutations in the three tested samples were built using Venny 2.1 [61]. Haplotype reconstruction was performed using seqPHASE [62] and PHASE [63,64]. The inferred haplotypes were analysed with DnaSP [65], which estimated the number of segregating sites and the level of nucleotide diversity π [66] in both synonymous and non-synonymous sites. Based on the number of segregating sites and sample size, we also manually

457 computed the nucleotide diversity estimator θ [67] and Tajima's *D* statistic [68]. We also tested for
458 signatures of adaptive evolution using the McDonald-Kreitman test [41], which compares the rate of
459 polymorphism and substitutions in synonymous and non-synonymous sites. For this analysis we
460 used alignments that included the orthologous sequences from *Ae. aegypti*.
461 Consensus sequences for each gene from each individual were also aligned in TranslatorX
462 [69] using Clustalw [70] and used for Maximum-likelihood based phylogenetic inference based on
463 RAxML after 1000 bootstrap under the GTRGAMMA model. Signs of selective pressure between
464 populations [71] were investigated with Codeml in PAML v. 4.9 [72], as implemented in PAMLX [73].
465 In particular, we compared the M1a (nearly-neutral) model to the M2a (positive selection) model by
466 inferring ω estimations and posterior probabilities under the Bayes empirical Bayes (BEB) approach
467 [72].
468 The overall level of polymorphism (LoP) for slow-evolving genes (SGs) (AALF008224,
469 AALF005886, AALF020750, AALF026109, AALF014156 , AALF018476, AALF014287,
470 AALF004102, AALF003606, AALF019476, AALF028431, AALF018378, AALF027761,
471 AALF014448), fast-evolving genes (FGs) (AALF010748, AALF022019, AALF024551, AALF017064,
472 AALF004733, AALF018679, AALF028390, AALF026991, AALF014993, AALF009493,
473 AALF010877, AALF012271, AALF009839, AALF019413) and the *Piwi* genes was calculated for
474 each population following the pipeline as in [42]. Briefly, SNPs and INDELs were inferred using four
475 Variant callers (i.e. Freebayes [58], Platypus [74], Vardict [75] and GATK UnifiedGenotyper [76]) and
476 the data merged and filtered with custom scripts. The LoP for each individual was calculated as the
477 number of variants averaged over the region length, and the median value for each population was
478 used for subsequent analyses. Statistical analyses were performed in R studio [77]. Fold-change
479 differences were computed as the ratio of the median LoP for each Piwi gene and each FG gene
480 over the median LoP of the SG genes. Statistical differences in LoP distribution was assessed via
481 the Kolmogorov-Smirnov test and the p-value threshold was adjusted with the Bonferroni correction.

Homology modelling

Computational structural investigations were carried out initially through the identification of the closest homologs based on sequence identity (using *NCBI Blast* [78]) and secondary structure matching (using *HHPRED* [79]). Homology model were then generated *MODELLER* [80] using on the structures *Kluyveromyces polysporus* Argonaute with a guide RNA (PDB ID 4F1N), Human Argonaute2 Bound to t1-G Target RNA (PDB ID 4z4d) [81], *T. thermophilus* Argonaute complexed with DNA guide strand and 19-nt RNA target strand (PDB ID 3HM9), and silkworm PIWI-clade Argonaute Siwi bound to piRNA (PDB ID 5GUH).

Computational models were manually adjusted through the removal of non-predictable N- and C-terminal flexible regions using *COOT* [82] followed by geometry idealization in *PHENIX* [83] to adjust the overall geometry. Final model quality was assessed by evaluating average bond lengths, bond angles, clashes, and Ramachandran statistics using Molprobity [84] and the *QMEAN* server [85] Structural figures were generated with *PyMol* [86].

Developmental expression profile of *Piwi* genes

Publicly available RNA-seq data (runs: SRR458468, SRR458471, SRR1663685, SRR1663700, SRR1663754, SRR1663913, SRR1812887, SRR1812889, SRR1845684) were downloaded and aligned using Burrows-Wheeler Aligner (BWA-MEM) [57] to the current *Ae. albopictus* genome assembly (AaloF1). Aligned reads were visualized in Integrative Genomics Viewer (IGV) [87]. Total RNA was extracted from embryos, 1st and 4th instar larvae, pupae, and adults using Trizol (Thermo Fisher Scientific). Embryos consisted of two pools of 60 eggs at different time points after oviposition (i.e. 4-8 h, 8-16 h and 16-24 h). Adult samples consisted of males and females kept on a sugar-diet; females fed an uninfected blood-meal; and females fed a DENV- or CHIK-infected blood. All blood-fed females were dissected to separate ovaries from the carcasses. Females fed an uninfected blood-meal were sampled 48 h after blood-meal. These parameters were based on the results of previous studies on *Anopheles stephensi* and *Ae. aegypti* that showed high *Piwi* gene expression during early embryogenesis or 48-72 h post blood meal [45]. For each stage,

508 RNA was extracted from pools of 10-15 mosquitoes, except for first instar larvae and embryos when
509 20 or 60 individuals were used, respectively.

510 RNA was DNaseI-treated (Sigma-Aldrich) and reverse-transcribed in a 20 µl reaction using
511 the qScript cDNA SuperMix (Quantabio) following the manufacturer's instructions. Quantitative RT-
512 PCRs (qRT-PCR) were performed as previously described using two biological replicates per
513 condition and the RPL34 gene as housekeeping [88]. Relative quantification of *Piwi* genes was
514 determined using the software qBase+ (Biogazelle). Expression values were normalized with respect
515 to those obtained from 4-8h embryos for the analysis of the developmental stages, and to sugar-fed
516 females for the infection analyses.

517 **Expression analyses following infection**

518 Fold-change expression values for each *Piwi* gene was assessed for non-infectious-blood-fed
519 controls, CHIKV-infected and DENV-infected samples after normalization on sugar-fed controls.
520 qRT-PCR experiments (Supplementary table 4) were set up for two replicate pools of 15 ovaries and
521 15 carcasses at days 4, 14 and 4, 21 for CHIKV and DENV, respectively and the corresponding
522 sugar and non-infectious-blood controls. RNA extraction, qRT-PCR and data analyses were
523 performed as described in the previous paragraph (see "Developmental expression profile of Piwi
524 genes"). Fold-change differences significance was assessed using the Analysis of Variance
525 (ANOVA) procedure [89,90] as implemented in qBASE+.

526

527 ## Funding

528 This research was funded by a European Research Council Consolidator Grant (ERC-CoG)
529 under the European Union's Horizon 2020 Programme (Grant Number ERC-CoG 682394) to M.B.;
530 by the Italian Ministry of Education, University and Research FARE-MIUR project R1623HZAH5 to
531 M.B.; by the Italian Ministry of Education, University and Research (MIUR): Dipartimenti Eccellenza
532 Program (2018–2022) Dept. of Biology and Biotechnology "L. Spallanzani", University of Pavia.

533

The funders had no role in study design, data collection and interpretation, or the decision to submit the work for publication.

Authors' contributions

MM performed all experiments, analyzed the data and wrote the manuscript; LH performed PCR and qRT-PCR analyses and analyzed the data; GI contributed in identifying *Ae. albopictus Piwi* genes and their transcript sequences; VH contributed in infection experiments and analyzed the data; FV contributed in characterizing *Piwi* gene transcripts and their expression; UP, LO and EP contributed in bioinformatic analyses for *Piwi* gene polymorphism; AF supervised infection experiments analyzed data and wrote the manuscript; JC performed WGS of wild-caught mosquitoes and revised the manuscript; FF performed computational homology modelling and structural analyses, and revised the manuscript; RCL contributed in collecting wild mosquitoes and analyzed the data; MB conceived the study, analyzed the data and wrote the manuscript. All authors read and approved the final manuscript.

Acknowledgments

We thank Monica Ruth Waghacore for insectary work.

References

1. Bohmert K, Camus I, Bellini C, Bouchez D, Caboche M, Banning C. AGO1 defines a novel locus of Arabidopsis controlling leaf development. EMBO J. 1998; doi:10.1093/emboj/17.1.170
2. Swarts DC, Makarova K, Wang Y, Nakanishi K, Ketting RF, Koonin E V., et al. The evolutionary journey of Argonaute proteins. Nature Structural and Molecular Biology. 2014. doi:10.1038/nsmb.2879
3. Lewis SH, Salmela H, Obbard DJ. Duplication and diversification of dipteran argonaute genes, and the evolutionary divergence of Piwi and Aubergine. Genome Biol Evol. 2016;8: 507–518. doi:10.1093/gbe/evw018
4. Buck AH, Blaxter M. Functional diversification of Argonautes in nematodes: an expanding universe: Figure 1. Biochem Soc Trans. 2013; doi:10.1042/BST20130086
5. Bollmann SR, Press CM, Tyler BM, Grünwald NJ. Expansion and divergence of argonaute genes in the oomycete genus phytophthora. Front Microbiol. 2018; doi:10.3389/fmicb.2018.02841
6. Singh RK, Gase K, Baldwin IT, Pandey SP. Molecular evolution and diversification of the Argonaute family of proteins in plants. BMC Plant Biol. 2015; doi:10.1186/s12870-014-0364-6
7. Bronkhorst AW, Van Rij RP. The long and short of antiviral defense: Small RNA-based immunity in insects. Current Opinion in Virology. 2014. doi:10.1016/j.coviro.2014.03.010
8. Poirier EZ, Goic B, Tomé-Poderti L, Frangeul L, Boussier J, Gausson V, et al. Dicer-2-Dependent Generation of Viral DNA from Defective Genomes of RNA Viruses Modulates Antiviral Immunity in Insects. Cell Host Microbe. 2018; doi:10.1016/j.chom.2018.02.001
9. Goic B, Stapleford KA, Frangeul L, Doucet AJ, Gausson V, Blanc H, et al. Virus-derived DNA drives mosquito vector tolerance to arboviral infection. Nat Commun. 2016; doi:10.1038/ncomms12410
10. Palatini U, Miesen P, Carballar-Lejarazu R, Ometto L, Rizzo E, Tu Z, et al. Comparative genomics shows that viral integrations are abundant and express piRNAs in the arboviral vectors Aedes aegypti and Aedes albopictus. BMC Genomics. 2017; doi:10.1186/s12864-017-3903-3
11. Whitfield ZJ, Dolan PT, Kunitomi M, Tassetto M, Seetin MG, Oh S, et al. The Diversity, Structure, and Function of Heritable Adaptive Immunity Sequences in the Aedes aegypti Genome. Curr Biol. 2017; doi:10.1016/j.cub.2017.09.067
12. Miesen P, Joosten J, van Rij RP. PIWIs Go Viral: Arbovirus-Derived piRNAs in Vector Mosquitoes. PLoS Pathog. 2016;12: 1–17. doi:10.1371/journal.ppat.1006017
13. Olson KE, Bonizzoni M. Nonretroviral integrated RNA viruses in arthropod vectors: an

occasional event or something more? Curr Opin Insect Sci. Elsevier Inc; 2017;22: 45–53. doi:10.1016/j.cois.2017.05.010

14. Brennecke J, Aravin AA, Stark A, Dus M, Kellis M, Sachidanandam R, et al. Discrete Small RNA-Generating Loci as Master Regulators of Transposon Activity in Drosophila. Cell. 2007;128: 1089–1103. doi:10.1016/j.cell.2007.01.043
15. Petit M, Mongelli V, Frangeul L, Blanc H, Jiggins F, Saleh M-C. piRNA pathway is not required for antiviral defense in *Drosophila melanogaster*. Proc Natl Acad Sci. 2016; doi:10.1073/pnas.1607952113
16. Akbari OS, Antoshechkin I, Amrhein H, Williams B, Diloreto R, Sandler J, et al. The Developmental Transcriptome of the Mosquito *Aedes aegypti* , an Invasive Species and Major Arbovirus Vector. G3: Genes|Genomes|Genetics. 2013; doi:10.1534/g3.113.006742
17. Matthews BJ, Dudchenko O, Kingan SB, Koren S, Antoshechkin I, Crawford JE, et al. Improved reference genome of Aedes aegypti informs arbovirus vector control. Nature. 2018; doi:10.1038/s41586-018-0692-z
18. Miesen P, Ivens A, Buck AH, van Rij RP. Small RNA Profiling in Dengue Virus 2-Infected Aedes Mosquito Cells Reveals Viral piRNAs and Novel Host miRNAs. PLoS Negl Trop Dis. 2016; doi:10.1371/journal.pntd.0004452
19. Girardi E, Miesen P, Pennings B, Frangeul L, Saleh MC, Van Rij RP. Histone-derived piRNA biogenesis depends on the ping-pong partners Piwi5 and Ago3 in Aedes aegypti. Nucleic Acids Res. 2017; doi:10.1093/nar/gkw1368
20. Miesen P, Girardi E, Van Rij RP. Distinct sets of PIWI proteins produce arbovirus and transposon-derived piRNAs in Aedes aegypti mosquito cells. Nucleic Acids Res. 2015;43: 6545–6556. doi:10.1093/nar/gkv590
21. Varjak M, Kean J, Vazeille M, Failloux A, Kohl A. Aedes aegypti Piwi4 Is a Noncanonical. mSphere. 2017;2: e00144-17.
22. Varjak M, Leggewie M, Schnettler E. The antiviral piRNA response in mosquitoes? 2018; 1–12. doi:10.1099/jgv.0.001157
23. Schnettler E, Donald CL, Human S, Watson M, Siu RWC, McFarlane M, et al. Knockdown of piRNA pathway proteins results in enhanced semliki forest virus production in mosquito cells. J Gen Virol. 2013;94: 1680–1689. doi:10.1099/vir.0.053850-0
24. Hahn MW. Distinguishing among evolutionary models for the maintenance of gene duplicates. Journal of Heredity. 2009. doi:10.1093/jhered/esp047
25. Obbard DJ, Jiggins FM, Halligan DL, Little TJ. Natural selection drives extremely rapid evolution in antiviral RNAi genes. Curr Biol. 2006;16: 580–585. doi:10.1016/j.cub.2006.01.065
26. Bonizzoni M, Gasperi G, Chen X, James AA. The invasive mosquito species Aedes

albopictus: Current knowledge and future perspectives. Trends in Parasitology. 2013. doi:10.1016/j.pt.2013.07.003

27. Rezza G. Dengue and chikungunya: long-distance spread and outbreaks in naïve areas. Pathog Glob Health. 2014; doi:10.1179/2047773214Y.0000000163

28. Bonilauri P, Bellini R, Calzolari M, Angelini R, Venturi L, Fallacara F, et al. Chikungunya virus in Aedes albopictus, Italy. Emerging Infectious Diseases. 2008. doi:10.3201/eid1405.071144

29. Venturi G, Di Luca M, Fortuna C, Elena Remoli M, Riccardo F, Severini F, et al. Detection of a chikungunya outbreak in Central Italy Detection of a chikungunya outbreak in Central. Euro Surveill. 2017;22: 1–4. doi:10.2807/1560

30. Gjenero-Margan I, Aleraj B, Krajcar D, Lesnikar V, Klobučar A, Pem-Novosel I, et al. Autochthonous dengue fever in Croatia, August- September 2010. Eurosurveillance. 2011;16: 1–4. doi:19805 [pii]

31. Marchand E, Prat C, Jeannin C, Lafont E, Bergmann T, Flusin O, et al. Autochthonous case of dengue in France, October 2013. Eurosurveillance. 2013; doi:10.2807/1560-7917.ES2013.18.50.20661

32. Delisle E, Rousseau C, Broche B, Leparc-Goffart I, L'Ambert G, Cochet A, et al. Chikungunya outbreak in Montpellier, France, September to October 2014. Euro Surveill. 2015; doi:10.2807/1560-7917.ES2015.20.17.21108

33. Calba C, Guerbois-Galla M, Franke F, Jeannin C, Auzet-Caillaud M, Grard G, et al. Preliminary report of an autochthonous chikungunya outbreak in France, July to September 2017. Eurosurveillance. 2017; doi:10.2807/1560-7917.ES.2017.22.39.17-00647

34. Bouri N, Sell TK, Franco C, Adalja AA, Henderson DA, Hynes NA. Return of epidemic dengue in the United States: Implications for the public health practitioner. Public Health Rep. 2012; doi:10.1177/003335491212700305

35. Joshua-Tor L. The argonautes. Cold Spring Harbor Symposia on Quantitative Biology. 2006. doi:10.1101/sqb.2006.71.048

36. Stone SS, Haldar JP, Tsao SC, Hwu W -m. W, Sutton BP, Liang Z-P. Accelerating advanced MRI reconstructions on GPUs. J Parallel Distrib Comput. 2008;68: 1307–1318. doi:10.1016/j.jpdc.2008.05.013

37. Yan KS, Yan S, Farooq A, Han A, Zeng L, Zhou M-M. Structure and conserved RNA binding of the PAZ domain. Nature. 2003; doi:10.1038/nature02129

38. Song JJ, Smith SK, Hannon GJ, Joshua-Tor L. Crystal structure of argonaute and its implications for RISC slicer activity. Science (80-). 2004; doi:10.1126/science.1102514

39. Cora E, Pandey RR, Xiol J, Taylor J, Sachidanandam R, McCarthy AA, et al. The MID-PIWI module of Piwi proteins specifies nucleotide- and strand-biases of piRNAs. RNA. 2014; doi:10.1261/rna.044701.114

40. Stein CB, Genzor P, Mitra S, Elchert AR, Ipsaro JJ, Benner L, et al. Decoding the 5′ nucleotide bias of PIWI-interacting RNAs. Nat Commun. Springer US; 2019;10: 828. doi:10.1038/s41467-019-08803-z
41. McDonald JH, Kreitman M. Adaptive protein evolution at the Adh locus in Drosophila. Nature. 1991; doi:10.1038/351652a0
42. Pischedda E, Scolari F, Valerio F, Carballar-Lejarazú R, Catapano PL, Waterhouse RM, et al. Insights Into an Unexplored Component of the Mosquito Repeatome: Distribution and Variability of Viral Sequences Integrated Into the Genome of the Arboviral Vector Aedes albopictus. Front Genet. 2019; doi:10.3389/fgene.2019.00093
43. Schirle NT, MacRae IJ. The crystal structure of human argonaute2. Science (80-). 2012; doi:10.1126/science.1221551
44. Matsumoto N, Nishimasu H, Sakakibara K, Nishida KM, Hirano T, Ishitani R, et al. Crystal Structure of Silkworm PIWI-Clade Argonaute Siwi Bound to piRNA. Cell. 2016; doi:10.1016/j.cell.2016.09.002
45. Macias V, Coleman J, Bonizzoni M, James AA. piRNA pathway gene expression in the malaria vector mosquito Anopheles stephensi. Insect Mol Biol. 2014;23: 579–586. doi:10.1111/imb.12106
46. Bonizzoni M, Dunn WA, Campbell CL, Olson KE, Marinotti O, James AA. Complex Modulation of the Aedes aegypti Transcriptome in Response to Dengue Virus Infection. PLoS One. 2012; doi:10.1371/journal.pone.0050512
47. Campbell CL, Keene KM, Brackney DE, Olson KE, Blair CD, Wilusz J, et al. Aedes aegypti uses RNA interference in defense against Sindbis virus infection. BMC Microbiol. 2008;8: 1–12. doi:10.1186/1471-2180-8-47
48. Hess AM, Prasad AN, Ptitsyn A, Ebel GD, Olson KE, Barbacioru C, et al. Small RNA profiling of Dengue virus-mosquito interactions implicates the PIWI RNA pathway in anti-viral defense. BMC Microbiol. 2011; doi:10.1186/1471-2180-11-45
49. La Ruche G, Souarès Y, Armengaud A, Peloux-Petiot F, Delaunay P, Desprès P, et al. First two autochthonous dengue virus infections in metropolitan France, september 2010. Eurosurveillance. 2010; doi:19676 [pii]
50. Schuffenecker I, Iteman I, Michault A, Murri S, Frangeul L, Vaney MC, et al. Genome microevolution of chikungunya viruses causing the Indian Ocean outbreak. PLoS Med. 2006; doi:10.1371/journal.pmed.0030263
51. Dubrulle M, Mousson L, Moutailier S, Vazeille M, Failloux AB. Chikungunya virus and Aedes mosquitoes: Saliva is infectious as soon as two days after oral infection. PLoS One. 2009; doi:10.1371/journal.pone.0005895
52. Campbell CL, Black IV WC, Hess AM, Foy BD. Comparative genomics of small RNA regulatory pathway components in vector mosquitoes. BMC Genomics. 2008;9.

doi:10.1186/1471-2164-9-425

53. Arensburger P, Hice RH, Wright JA, Craig NL, Atkinson PW. The mosquito Aedes aegypti has a large genome size and high transposable element load but contains a low proportion of transposon-specific piRNAs. BMC Genomics. 2011;12. doi:10.1186/1471-2164-12-606

54. Yuan JS, Burris J, Stewart NR, Mentewab A, Neal CN. Statistical tools for transgene copy number estimation based on real-time PCR. BMC Bioinformatics. 2007;8: 1–12. doi:10.1186/1471-2105-8-S7-S6

55. Baruffi L, Damiani G, Guglielmino CR, Bandii C, Malacrida AR, Gasperi G. Polymorphism within and between populations of ceratitis: Comparison between RAPD and multilocus enzyme electrophoresis data. Heredity (Edinb). 1995;74: 425–437. doi:10.1038/hdy.1995.60

56. Edgar RC. MUSCLE: Multiple sequence alignment with high accuracy and high throughput. Nucleic Acids Res. 2004; doi:10.1093/nar/gkh340

57. Li H. Aligning sequence reads, clone sequences and assembly contigs with BWA-MEM. 2013; Available: https://arxiv.org/abs/1303.3997

58. Garrison E, Marth G. Haplotype-based variant detection from short-read sequencing -- Free bayes -- Variant Calling -- Longranger. arXiv Prepr arXiv12073907. 2012; doi:arXiv:1207.3907 [q-bio.GN]

59. Cingolani P, Platts A, Wang LL, Coon M, Nguyen T, Wang L, et al. A program for annotating and predicting the effects of single nucleotide polymorphisms, SnpEff: SNPs in the genome of Drosophila melanogaster strain w1118; iso-2; iso-3. Fly (Austin). 2012; doi:10.4161/fly.19695

60. Schroeder MP, Lopez-Bigas N. muts-needle-plot: Mutations Needle Plot v0.8.0. 2015; doi:10.5281/ZENODO.14561

61. Oliveros JC. Venny. An interactive tool for comparing lists with Venn﷽s diagrams. 2007--2015. h ttp. bioinfogp cnb csic es/tools/venny/index html Accessed. 2016;

62. Flot JF. Seqphase: A web tool for interconverting phase input/output files and fasta sequence alignments. Mol Ecol Resour. 2010; doi:10.1111/j.1755-0998.2009.02732.x

63. Stephens M, Smith NJ, Donnelly P. A new statistical method for haplotype reconstruction from population data. Am J Hum Genet. 2001; doi:10.1086/319501

64. Stephens M, Scheet P. Accounting for Decay of Linkage Disequilibrium in Haplotype Inference and Missing-Data Imputation. Am J Hum Genet. 2005; doi:10.1086/428594

65. Librado P, Rozas J. DnaSP v5: A software for comprehensive analysis of DNA polymorphism data. Bioinformatics. 2009; doi:10.1093/bioinformatics/btp187

66. Tajima F. Evolutionary relationship of DNA sequences in finite populations. Genetics. 1983;

67. Watterson GA. On the number of segregating sites in genetical models without recombination. Theor Popul Biol. 1975; doi:10.1016/0040-5809(75)90020-9

68. Tajima F. Statistical method for testing the neutral mutation hypothesis by DNA

polymorphism. Genetics. 1989;

69. Abascal F, Zardoya R, Telford MJ. TranslatorX: Multiple alignment of nucleotide sequences guided by amino acid translations. Nucleic Acids Res. 2010; doi:10.1093/nar/gkq291

70. Thompson JD, Higgins DG, Gibson TJ. CLUSTAL W: Improving the sensitivity of progressive multiple sequence alignment through sequence weighting, position-specific gap penalties and weight matrix choice. Nucleic Acids Res. 1994; doi:10.1093/nar/22.22.4673

71. Bernhardt SA, Simmons MP, Olson KE, Beaty BJ, Blair CD, Black WC. Rapid Intraspecific Evolution of miRNA and siRNA Genes in the Mosquito Aedes aegypti. PLoS One. 2012;7. doi:10.1371/journal.pone.0044198

72. Yang Z. PAML 4: Phylogenetic analysis by maximum likelihood. Mol Biol Evol. 2007; doi:10.1093/molbev/msm088

73. Xu B, Yang Z. PamlX: A graphical user interface for PAML. Mol Biol Evol. 2013; doi:10.1093/molbev/mst179

74. Rimmer A, Phan H, Mathieson I, Iqbal Z, Twigg SRF, Wilkie AOM, et al. Integrating mapping-, assembly- and haplotype-based approaches for calling variants in clinical sequencing applications. Nat Genet. 2014; doi:10.1038/ng.3036

75. Lai Z, Markovets A, Ahdesmaki M, Chapman B, Hofmann O, Mcewen R, et al. VarDict: A novel and versatile variant caller for next-generation sequencing in cancer research. Nucleic Acids Res. 2016; doi:10.1093/nar/gkw227

76. McKenna A, Hanna M, Banks E, Sivachenko A, Cibulskis K, Kernytsky A, et al. The Genome Analysis Toolkit: a MapReduce framework for analyzing next-generation DNA sequencing data. Genome Res. 2010; doi:10.1101/gr.107524.110

77. Rstudio Team. RStudio: Integrated Development for R. [Online] RStudio, Inc., Boston, MA. 2016. doi:10.1007/978-81-322-2340-5

78. Altschul SF, Gish W, Miller W, Myers EW, Lipman DJ. Basic local alignment search tool. J Mol Biol. 1990; doi:10.1016/S0022-2836(05)80360-2

79. Zimmermann L, Stephens A, Nam SZ, Rau D, Kübler J, Lozajic M, et al. A Completely Reimplemented MPI Bioinformatics Toolkit with a New HHpred Server at its Core. J Mol Biol. 2018; doi:10.1016/j.jmb.2017.12.007

80. Webb B, Sali A. Protein structure modeling with MODELLER. Methods in Molecular Biology. 2017. doi:10.1007/978-1-4939-7231-9_4

81. Schirle NT, Sheu-Gruttadauria J, Chandradoss SD, Joo C, MacRae IJ. Water-mediated recognition of t1-adenosine anchors Argonaute2 to microRNA targets. Elife. 2015; doi:10.7554/elife.07646

82. Emsley P, Lohkamp B, Scott WG, Cowtan K. Features and development of Coot . Acta Crystallogr Sect D Biol Crystallogr. 2010; doi:10.1107/s0907444910007493

83. Adams PD, Afonine P V., Bunkóczi G, Chen VB, Echols N, Headd JJ, et al. The Phenix

772 software for automated determination of macromolecular structures. Methods. 2011.
773 doi:10.1016/j.ymeth.2011.07.005
774 84. Williams CJ, Headd JJ, Moriarty NW, Prisant MG, Videau LL, Deis LN, et al. MolProbity:
775 More and better reference data for improved all-atom structure validation. Protein Sci. 2018;
776 doi:10.1002/pro.3330
777 85. Benkert P, Künzli M, Schwede T. QMEAN server for protein model quality estimation.
778 Nucleic Acids Res. 2009; doi:10.1093/nar/gkp322
779 86. Schrödinger L. The PyMOL molecular graphics system, version 1.8.
780 https://www.pymol.org/citing. 2015;
781 87. Robinson JT, Thorvaldsdóttir H, Winckler W, Guttman M, Lander ES, Getz G, et al.
782 Integrative genomics viewer. Nature Biotechnology. 2011. doi:10.1038/nbt.1754
783 88. Reynolds JA, Poelchau MF, Rahman Z, Armbruster PA, Denlinger DL. NIH Public Access.
784 2013;58: 966–973. doi:10.1016/j.jinsphys.2012.04.013.Transcript
785 89. Khan A, Rayner GD. Robustness to non-normality of common tests for the many-sample
786 location problem. J Appl Math Decis Sci. 2004; doi:10.1155/S1173912603000178
787 90. Blanca MJ, Alarcón R, Arnau J, Bendayan R. Non-normal data: Is ANOVA still a valid
788 option? Psicothema. 2017; doi:10.7334/psicothema2016.383
789 91. Ashkenazy H, Erez E, Martz E, Pupko T, Ben-Tal N. ConSurf 2010: Calculating evolutionary
790 conservation in sequence and structure of proteins and nucleic acids. Nucleic Acids Res.
791 2010; doi:10.1093/nar/gkq399
792 92. Madeira F, Park, Y M, Lee J, Buso N, Gur T, Madhusoodanan N, et al. The EMBL-EBI
793 search and sequence analysis tools APIs in 2019. Nucleic Acids Res. 2019;
794 93. Robert X, Gouet P. Deciphering key features in protein structures with the new ENDscript
795 server. Nucleic Acids Res. 2014; doi:10.1093/nar/gku316
796
797

Figure legends

Figure 1. Gene and transcript structure of *Ae. albopictus Piwi5* and *Piwi7*. A) Schematic representation of the DNA structure of *Piwi5* and *Piwi7* genes and their corresponding transcripts as obtained from cDNA amplification of single sugar-fed mosquito samples. Exons and introns are shown by blue boxes and black lines, respectively, with corresponding length in nucleotide below each. The positions of the predicted PAZ, MID and PIWI domains are shown by green, blue and magenta ovals, respectively. Exon numbers correspond to lane numbers. B) Amplification of each exon of Piwi5 and Piwi7 on genomic DNA. Exon numbers correspond to lane numbers. C) Northern-blot results of *Piwi5* indicate the presence of a transcript of 3 kb.

Figure 2. Venn diagrams showing the number of positions harbouring synonymous and non-synonymous mutations in tested samples for each *Piwi* gene.

Figure 3. Volcano plot. Level of polymorphism (LoP) comparison between slow-evolving genes (SGs), fast-evolving genes (FGs) and *Piwi* genes by population. Genes on the right side of the panel have LoP values greater than those of SGs, while genes on the left side have LoPs smaller than SGs. The y-axis represents the -log10 p-values of the Kolmogorov-Smirnov test. Faint datapoints are not significant after Bonferroni correction for multiple testing (-log10 0.0024 (0.05/21 genes) = 2.62).

Figure 4. Computational homology models of the *Ae. Albopictus Piwi* proteins. Homology models were generated for the seven *Piwi* genes as described in the methods section. A) Superposition of cartoon representations of Piwi homology models, with highlight of domain organization: the N-terminal domain is shown in orange, the PAZ domain in green, the MID domain in blue and the PIWI domain in magenta. B) *CONSURF* [91]overview of the amino acid sequence conservation mapped on three-dimensional homology models in a putative RNA-bound arrangement based on the structure of human Argonaute bound to a target RNA (PDB ID 4Z4D), coloured from teal (very low conservation) to dark magenta (highly conserved).

Figure 5. Expression profile of *Piwi* genes. Heatmap representations of log10 transformed fold-change expression values of each *Piwi* gene. A) Developmental expression pattern of the *Piwi*

825 genes normalized on expression in early embryos (4-8h). B) Expression pattern of *Piwi* genes
826 following viral infection normalized with respect to sugar-fed samples. Expression was verified in
827 ovaries and carcasses separately, during the early and late stages of infections, that is 4 days post
828 infection for both viruses and 14 or 21 dpi for CHIKV and DENV, respectively. Each day post
829 infection was analysed with respect to sugar and blood-fed controls of the same day. * indicates
830 significant difference ($P<0.05$) between infected samples and the corresponding blood-fed control.

831 **Fig. 1**

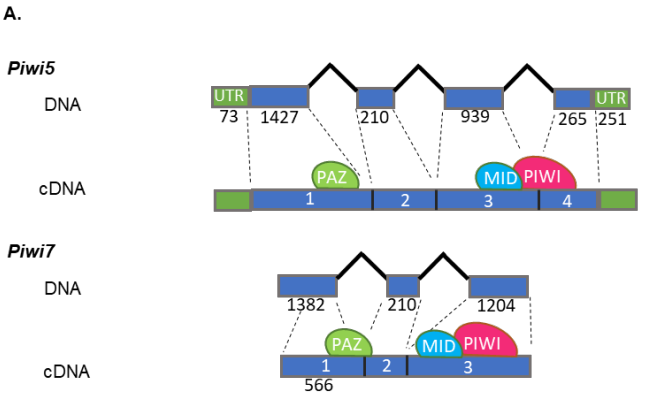

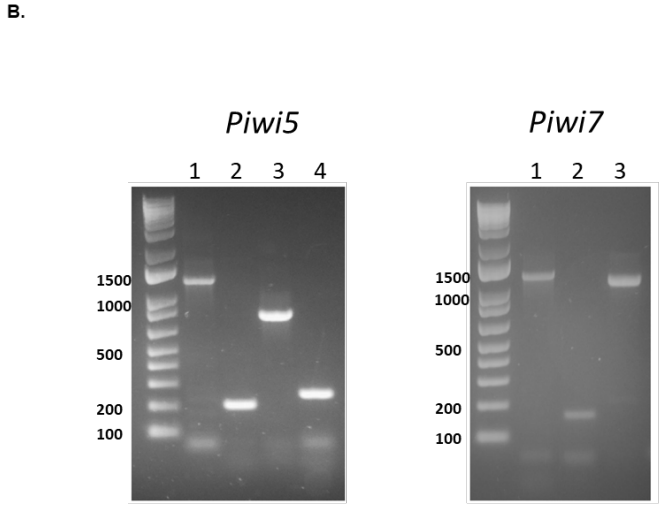

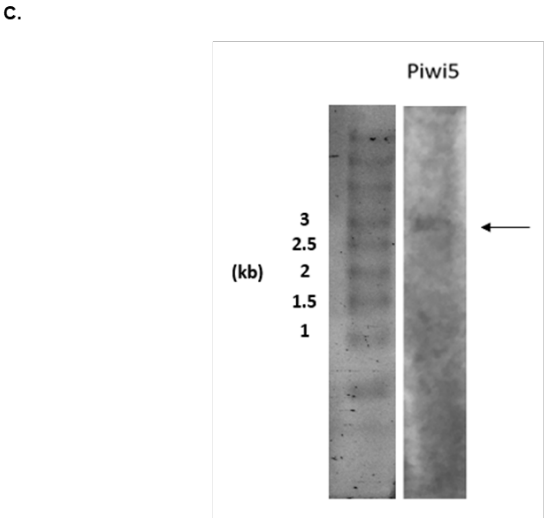

832 **Fig. 2**

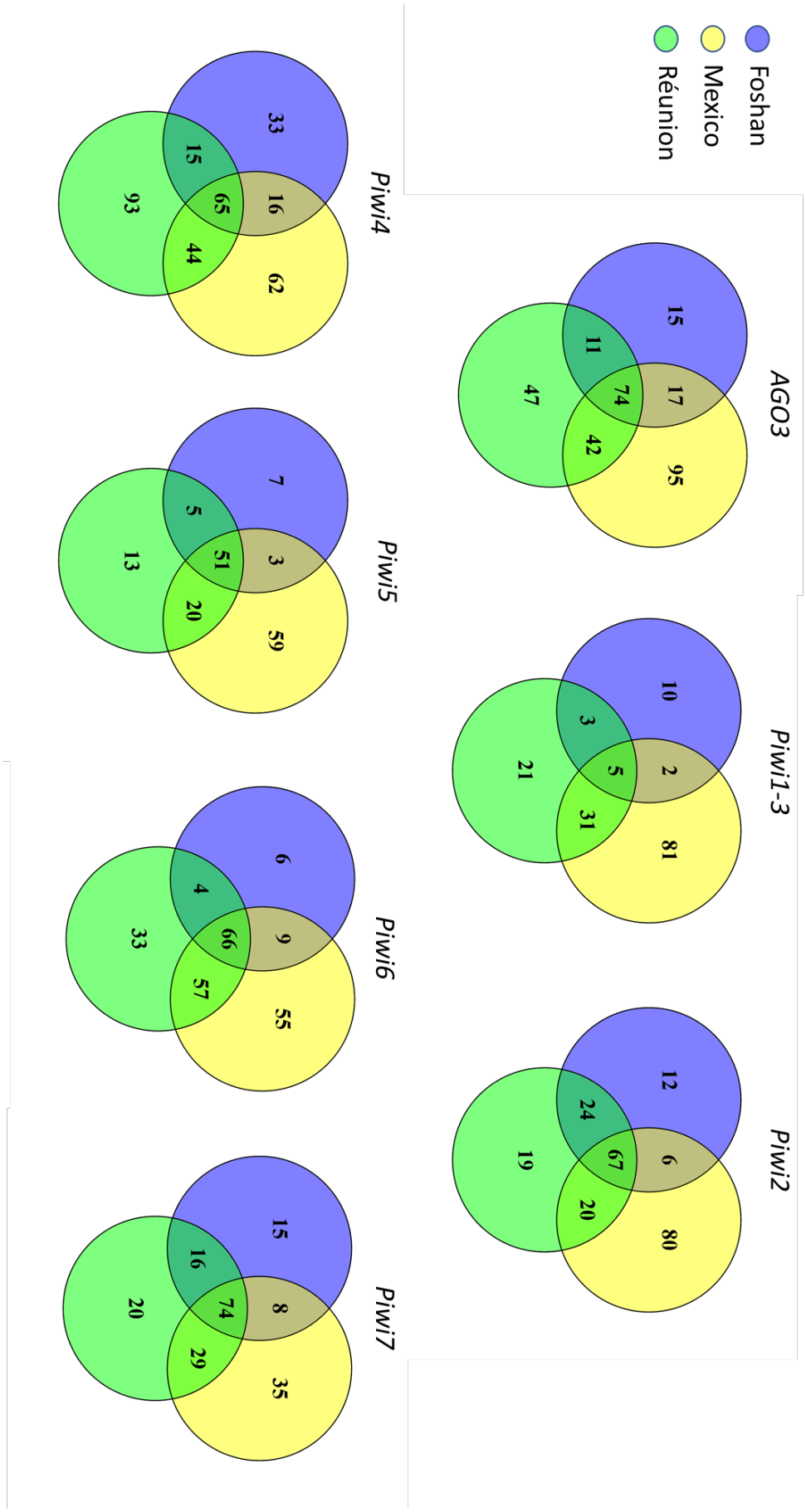

833 **Fig. 3**

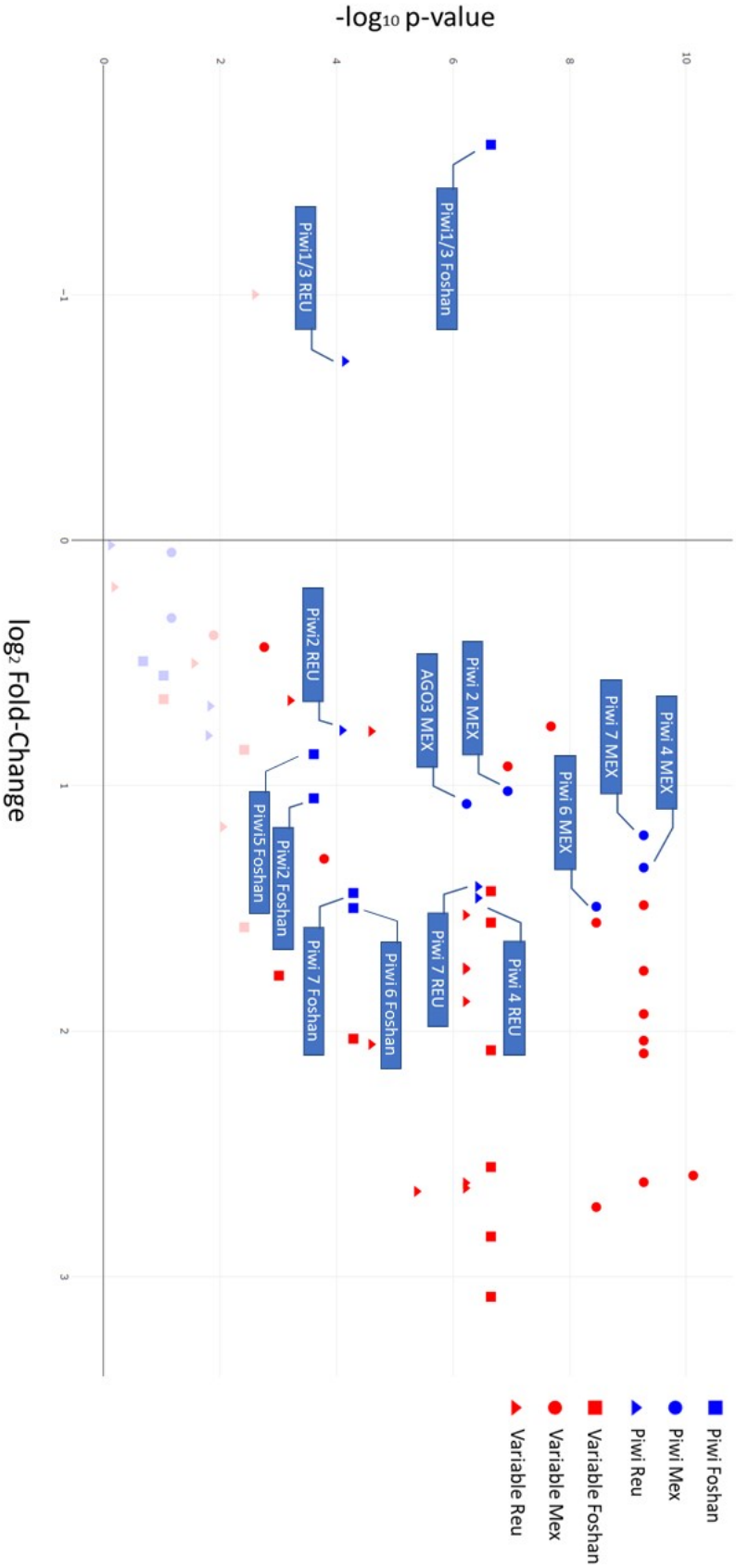

834 **Fig. 4**

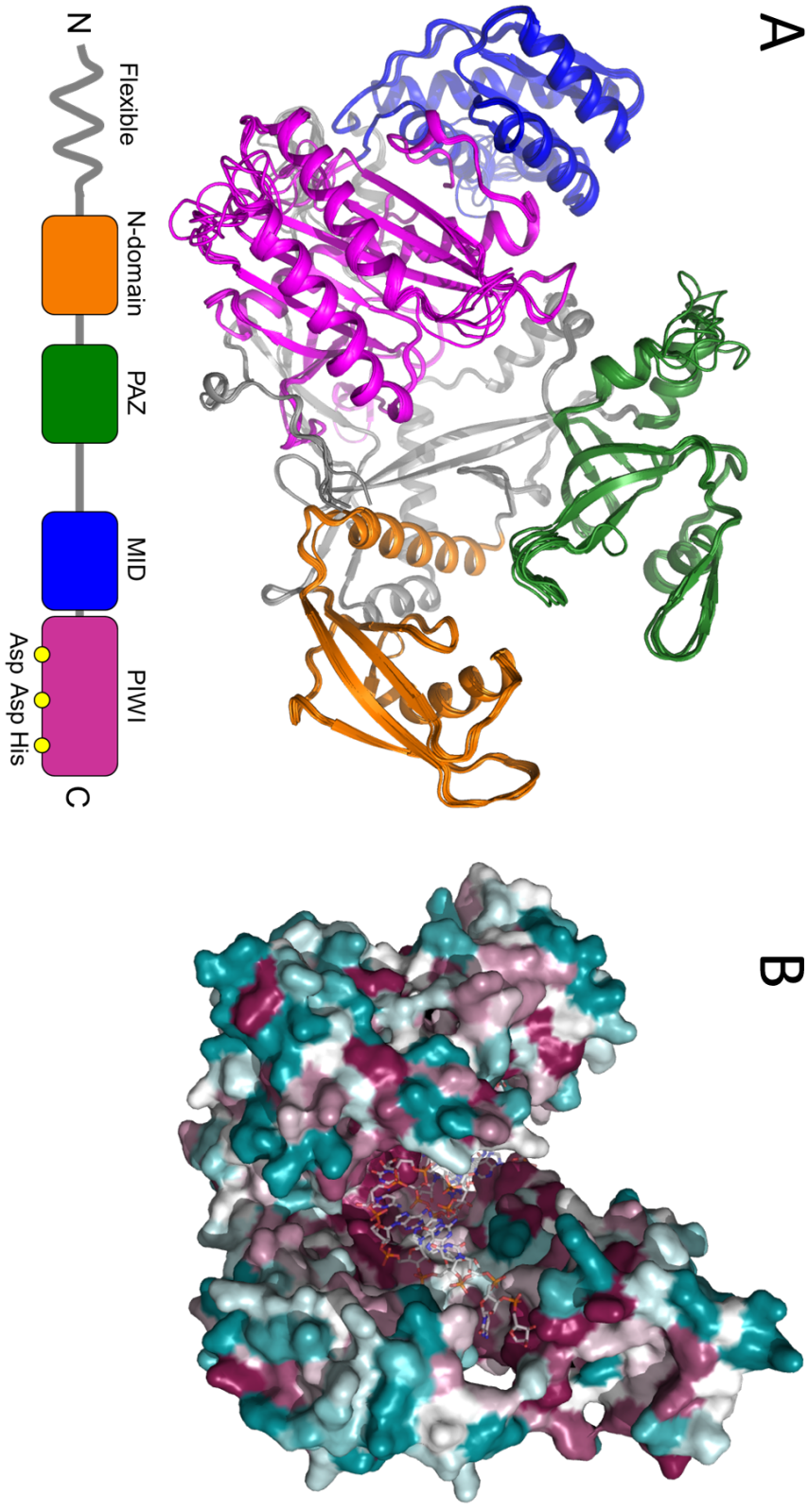

835 **Fig. 5**

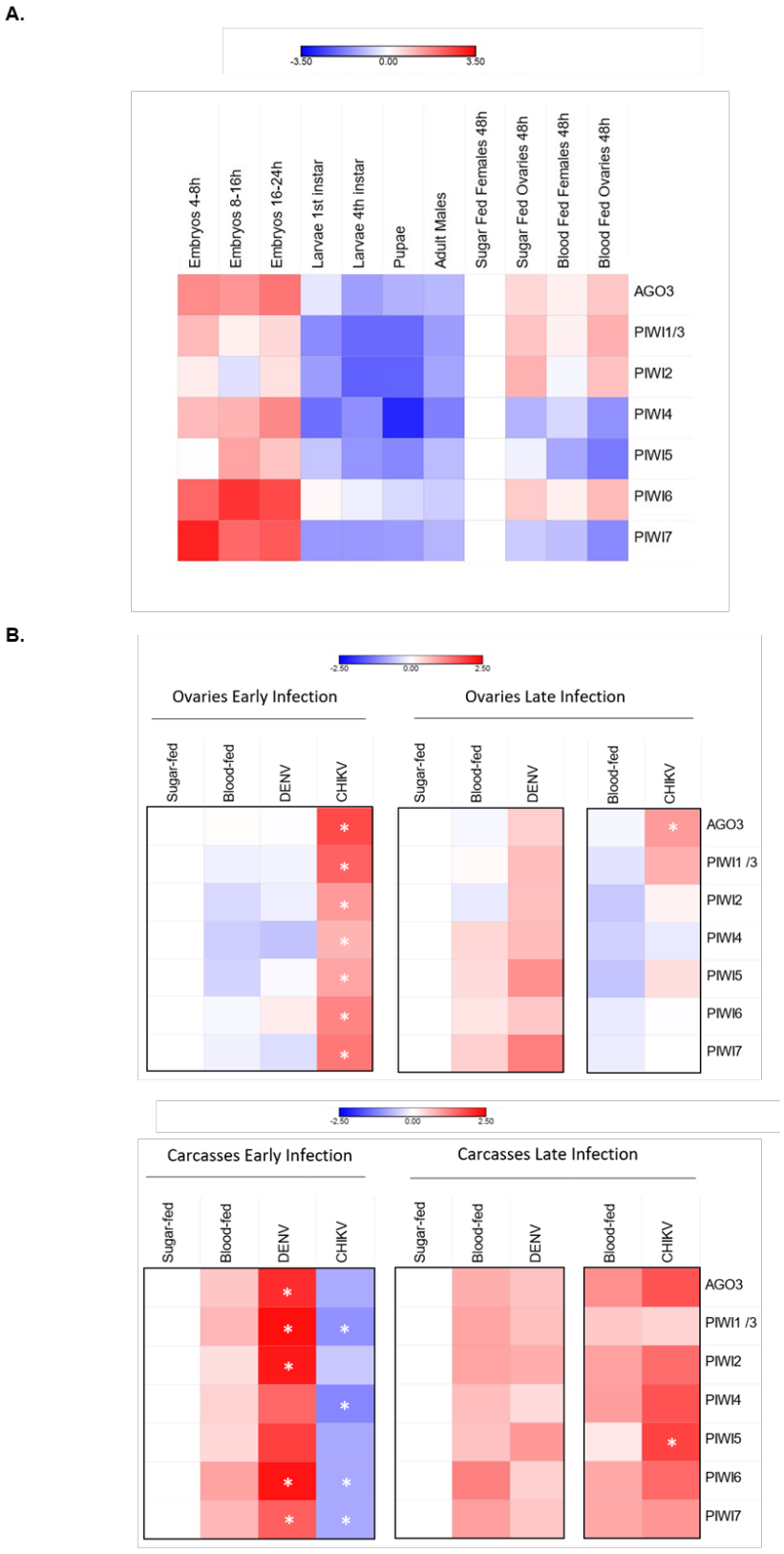

Supporting information

S1 Table. List of the core components of the piRNA pathway in *Ae. aegypti* and their orthologous in *Ae. albopictus.*

S2 Table. List of Transcript IDs and abbreviations of the Culicidae and Drosophilidae species included in the phylogenetic analyses.

S3 Table. Number of non-synonymous mutations found in mosquitoes of the Foshan strain (Foshan) and wild-caught samples from Mexico (Mex) and the island of La Reunion (Reu) divided by type (i.e. missense [M] , frameshift [F], indel [I] and nonsense [N]) and number of sites in which

S4 Table. Relative expression values (log10 fold-change) of Piwi genes during development (A) and following viral infection (B) normalized with respect to sugar-fed samples. Samples (2 pools per condition, 15 individuals each) were analysed at 4 days post infection (early infection) and at 14 and 21 days post infection for CHIKV and DENV, respectively (late infection). Each condition was normalized to the corresponding Sugar-fed control and compared to the corresponding Blood-fed control. Ovaries and carcasses were analysed independently. * indicates statistically significant difference between infected and non-infected blood-fed samples (ANOVA framework). Relative expression values may mask differences in levels of expression. For instance, the Ct values of Piwi6, Piwi7 and Piwi1/3 in ovaries 4 days post infection with CHIKV were 30, 33.39 and 25.20, respectively. Ovaries of blood-fed samples at the same time point showed Ct values of 30.30, 33.93 and 26.55 for Piwi6, Piwi7 and Piwi1/3. When relative expression was calculated with respect to Ct values of RPL34, fold-changes in gene expression were comparable among the three genes in both conditions, but Ct values clearly indicate that Piwi7 is less expressed than both Piwi1/3 and Piwi6. These considerations were taken into account when describing results.

S5 Table. List of primers used for CDS analyses, copy number estimation, qPCR experiments and Northern Blot probe design.

S1 Dataset. CDS of the seven *Piwi* genes of *Ae. albopcitus*. The sequence of the **PAZ**, MID and ***PIWI*** domains is in **bold**, underline and ***bold-italics***, respectively.

862 **S1 Fig. Maximum likelihood cladogram generated from the alignment of transcript sequences**
863 **of annotated *Piwi* genes in Culicinae.** Transcript IDs and species abbreviations are as listed in S2
864 Table. AlbPiwi3 is the same as Piwi1/3 in the text. *Piwi* gene transcripts from *Ae. albopictus* are in
865 red, from *Ae. aegypti* in purple, from *Culex quinquefasciatus* in pink. Transcripts from *D.*
866 *melanogaster Ago3*, *Piwi* and *Aubergine* genes are included for reference and shown in blue. All
867 nodes were supported by bootstrap values higher than 50% with the exception of the three nodes
868 with a black dot.
869 **S2 Fig. Polymorphism of *Piwi4* and *Piwi5*.** Lollipop plots representing position, amount and type
870 of mutation along the coding sequences of *Piwi4* and *Piwi5* in mosquitoes of the Foshan strain, from
871 la Reunion Island (Reu) and Mexico (Mex) as inferred by Freebayes and SnpEFF analyses. Only
872 missense (blue), nonsense (red) and indels (orange) and frameshift (yellow) are shown. The PAZ,
873 MID and PIWI domains are shown in green, blue and magenta, respectively. DDH residues positions
874 are highlighted in the PIWI domain.
875 **S3 Fig.** Sequence alignment of *Aedes albopictus* Piwi proteins. Domain boundaries inferred from
876 structural predictions are highlighted by coloured lines using the same colour coding as in figure 4
877 (Orange: N-terminus; Green: PAZ; Blue: MID; Magenta: PIWI). Conserved DDH residues found in
878 PIWI are indicated by (▲). The “acc” line indicates relative solvent accessibility, ranging from blue
879 (accessible) to white (buried). The sequence alignment was generated using EBI muscle [92] and
880 depicted using ESPRIPT3 [93]
881